Simplified Design of Common-Mode Chokes for Reduction of Motor Ground Currents in Inverter Drives

A. Muetze
C. R. Sullivan

Found in *IEEE Industry Applications Society Annual Meeting,* Oct. 2006, pp. 2304–2311.

Simpli ed Design of Common-Mode Chokes for Reduction of Motor Ground Currents in Inverter Drives

Annette Muetze
Dept. of Electrical and Computer Engineering
University of Wisconsin Madison, Madison, WI 53706 USA
muetze@engr.wisc.edu

Charles R. Sullivan
Thayer School of Engineering
Dartmouth College, Hanover, NH 03755 USA
chrs@dartmouth.edu http://power.thayer.dartmouth.edu

Abstract **A simpli ed design calculation for common-mode chokes for reducing motor ground currents provides insight on the effects of various parameters and allows easy design. Key simplifying assumptions are that the voltage rise time is short compared to the ring period and that the damping is small. Example designs for machines up to 450mm frame size show how effective ground-current reduction is possible with small, inexpensive, single-turn chokes.**

I. Introduction

The high-frequency (HF) ground current that can occur in inverter-based drive systems can cause different parasitic phenomena. Depending on the overall system, notably the drive size and presence of additional mitigation techniques, these parasitic phenomena can lead to early drive failure due to HF circulating bearing currents and bearing currents due to rotor ground currents, wide band EMI, and interference with ground fault protection systems in industrial facilities, to name some [1] [9]. Common-mode chokes that are placed in the inverter-output (Fig. 1) can be a cost-effective method of reducing such ground currents in motors used with PWM drive systems [4], [6] [8]. Because of the interaction between the circuit waveforms, the choke value, the possible use of the motor-inverter interconnect cables, and the large current magnitude, the requirements for such chokes differ from standard choke design [10]. Because of the large size of the motor leads of higher-power drives, feed-through chokes with only one turn are more easily installed than wound chokes. More complicated structures, such as *lter s* that provide a connection to the inverter-dc link, are beyond the scope of this contribution.

II. Design Approach: Simplifying Assumptions

We model the circuit as a simple series LRC circuit (similar to what is done in [4], [6]) with an input that ramps rapidly from one constant voltage to another, at each switching transition. Each switching transition is analyzed independently. This approach is justi ed as the ring period is long compared to the transition time, particularly with large drives and with effectively used common-mode chokes [10].

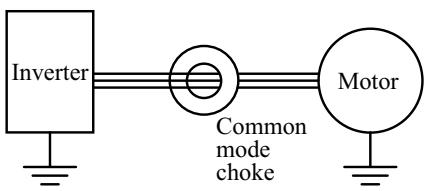

Fig. 1. Simpli ed sketch to illustrate placement of common mode choke in the inverter-output.

If the ring period is long compared to the transition time, the slope dv/dt has little bearing on the ground current, and we can simplify the analysis by assuming an instantaneous step in the input voltage (in nite dv/dt). Although the assumption of a short transition time is not always accurate in practice, it can be a useful simplifying assumption which facilitates analytical design equations which give general guidance to designers. We proceed with design using this assumption. Simulation results in Section V con rm that the error introduced is small.

The analysis also depends on the resistance value and the degree of damping. As the inductance is increased, the damping is decreased, assuming the losses in the inductor itself are small. Thus, we are typically interested in low-damping cases. Exemplarily, Fig. 2 shows the dependency of the peak current on the inductance value for different capacitance values $dv/dt = 2\text{kV}/\mu\text{s}$, and $R = 1\Omega$ (simulation results). As the low-damping case is also the worst-case situation, it is reasonable to limit the analysis to this situation.

With the assumptions of a common-mode step input of amplitude ΔV and light damping, a design that does not saturate will limit the peak ground current (common-mode) to approximately

$$I_{peak} \approx \Delta V / \sqrt{L/C} \tag{1}$$

Although this simpli ed analysis will not hold for all designs, it will hold for the designs we wish to choose, so we can proceed with the choke design based on (1).

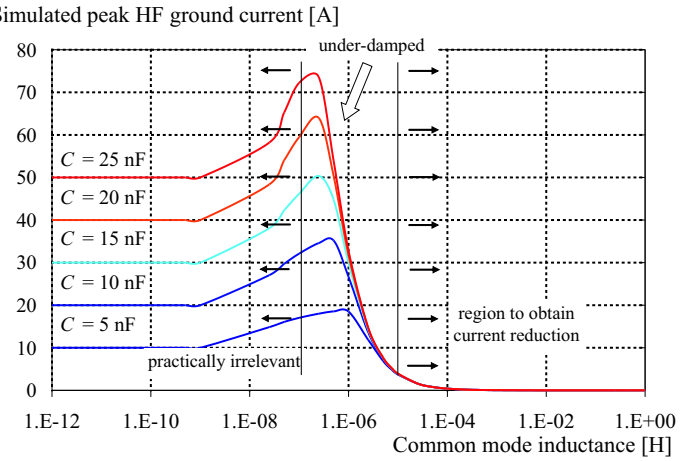

Fig. 2. Dependency of peak current on inductance values, for different capacitance values $dv/dt = 2\text{kV}/\mu\text{s}, R = 1\Omega$.

1-4244-0365-0/06/$20.00 (c) 2006 IEEE

III. Choke Design

We proceed to design a choke based on (1). The choke must achieve the required inductance:

$$L = \left(\frac{\Delta V}{I_{peak}}\right)^2 C \tag{2}$$

which we equate to the inductance for a given core geometry

$$L = \frac{N^2 \mu A_c}{\ell_c} = \left(\frac{\Delta V}{I_{peak}}\right)^2 C \tag{3}$$

where ℓ_c is the circumferential length, A_c the cross sectional area (Fig. 3), μ the permeability, and N the number of turns. Note that $A_c = ab$ is the cross sectional area that can be given by any aspect ratio $a : b$.

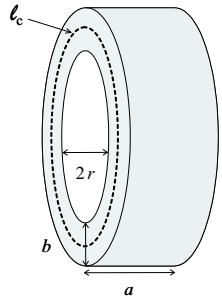

Fig. 3. Toroid nomenclature.

We now have a specification for the inductance and a specification for the peak current, which is sufficient information to use with any standard inductor design procedure. However, proceeding with the analysis of this particular case is important for two reasons.

1) We wish to develop equations that directly show how the parameters of the application, ΔV, C, and I_{peak}, affect the inductor design.
2) The inductor may be wound with the cable used to connect the inverter to the motor, which changes the design considerations relative to those for a typical inductor wound from wire chosen for the inductor. In this case, the wire diameter is fixed, and it is also desirable to use only a single turn.

The next step in completing an inductor design is to consider flux density, which may in general be limited by saturation or by core loss. Since the common-mode currents are in the form of short spikes, we assume that saturation, rather than core loss, is the relevant constraint. This constraint can be examined through a direct calculation of the peak flux density, or by considering energy storage. Either leads to the same results; we choose to consider energy. The core may or may not be gapped, but we unify the treatment by considering gapped cores in terms of an effective permeability $\mu_{eff} = \mu$. Equating the required energy storage to the actual energy storage results in

$$\frac{1}{2} L I_{peak}^2 = \frac{1}{2} \int B_{peak} H dv. \tag{4}$$

Assuming uniform flux density throughout the core, and linear magnetics, we have

$$L I_{peak}^2 = \frac{B_{peak}^2}{\mu} A_c \ell_c. \tag{5}$$

Solving for the volume (approximated by $A_c \ell_c$) and using (3) we obtain

$$A_c \ell_c = C \mu \frac{(\Delta V)^2}{B_{peak}^2}. \tag{6}$$

Although (6) is an appealingly simple equation, it is potentially misleading it might seem to indicate that the use of low permeability would enable the use of arbitrarily small volume cores. However, such a design would need to have a very small window area, and the required fine wire would have excessive resistance and would overheat. (In the limit, the design would be a short length of ultra fine wire which has high inductance per unit length, but very little current carrying capability.)

Thus, we must also consider the window area available for the winding, which, for a circular window of a toroidal core, is $A_w = \pi r^2$, where r is the window radius. As we are seeking to develop design equations that give general guidance to designers we are simplifying $2\pi r \approx \ell_c$ thus $r \approx \ell_c/(2\pi)$, where the error introduced will depend on how the cross sectional area $A_c = ab$ is being realized. Then,

$$A_w \approx \frac{\ell_c^2}{4\pi} = \mu^2 \frac{N^2 I_{peak}^2}{4\pi B_{peak}^2} \tag{7}$$

which directly shows that a small permeability μ will require a vanishingly small window area to meet the specifications.

Assuming we have control of the permeability value (either through selection of the core or gapping), a smaller window size is desirable insofar as it is feasible. So it is necessary to establish a minimum window size to proceed with the design. This depends on the wire used to wind the choke and the number of turns. The simplest option is to wind the choke with the same wires used to connect the inverter to the machine, and we consider this case first. Note also that the approach includes both multi-turn wound chokes and the more easily installed single-turn feed-through chokes.

A. Case 1: Fixed wire diameter; free choice of μ

Consider winding the choke with the machine lead wire connecting the inverter to the machine, which has outside diameter d_o, including insulation, per-phase. The required window area is, for three phase wires,

$$A_w = \frac{3\pi N d_o^2}{4F_p} \tag{8}$$

where F_p is a packing factor, defined as ratio of the wire area (including insulation) to the core window area. For a circular window, the maximum packing factor can be calculated from

simple geometrical considerations to be

$$\begin{aligned} F_{p,max} &= \frac{3\pi(d_o/2)^2}{A_w} \\ &= \frac{3\pi(d_o/2)^2}{\pi(d_o/2)^2(1+1/(\sqrt{3}/2))^2} \\ &= \frac{9}{(\sqrt{3}+2)^2} \approx 0.646. \end{aligned} \tag{9}$$

From (7) and (8), we obtain

$$\frac{\ell_c^2}{4\pi} = \frac{3\pi N d_o^2}{4F_p} \tag{10}$$

$$\ell_c = \pi d_o \sqrt{\frac{3}{F_p}}\sqrt{N} \tag{11}$$

We de ne a constant $k_w = \pi d_o \sqrt{\frac{3}{F_p}}$ to enable writing this more simply as

$$\ell_c = k_w \sqrt{N}. \tag{12}$$

This result can be used with (12) to establish

$$\mu = k_w \frac{B_{peak}}{\sqrt{N} I_{peak}}. \tag{13}$$

Using this value of permeability in (6), we obtain an expression for magnetic volume:

$$A_c \ell_c = \frac{(\Delta V)^2}{B_{peak}} \frac{C}{I_{peak}} \frac{k_w}{\sqrt{N}} \tag{14}$$

or, writing out k_w explicitly,

$$A_c \ell_c = \frac{(\Delta V)^2}{B_{peak}} \frac{C}{I_{peak}} \pi d_o \sqrt{\frac{3}{F_p}} \frac{1}{\sqrt{N}}. \tag{15}$$

The core size as expressed by either (14) or (15) appears dramatically different from standard inductor sizing equations, which typically show the size as proportional to LI^2, with a x ed temperature rise (the Hanna-curve method [11]) or a x ed Q value (the K_g method [12]). The dependence on L in (14) and (15) is hidden, instead, the result is written in terms of the performance and application speci cations. The dependence on current is different because it is assumed that I_{peak} is in effect for a short enough time that the winding dissipation associated with it is insigni cant.

Based on the above analysis, we can completely specify the design with

$$\ell_c = \pi d_o \sqrt{\frac{3}{F_p}}\sqrt{N} \tag{16}$$

$$A_c = \frac{(\Delta V)^2}{B_{peak}} \frac{C}{I_{peak}} \frac{1}{N} \tag{17}$$

$$\mu_{ideal} = \frac{\pi d_o \sqrt{\frac{3}{F_p}}}{\sqrt{N} I_{peak} B_{peak}} \tag{18}$$

From these equations we can draw several conclusions:

- A high packing factor is preferred; *i.e.*, for a given wire diameter, one should ordinarily use the minimum core window size that the wire will t through. The core size is reduced by a high packing factor (15), as is the required permeability. An exception to this rule is if the permeability found from (18) was *lower* than available permeabilities, and gapping was not practical. This situation is addressed in Section III-C. However, if the *ideal* permeability μ_{ideal} found from (18) is *higher* than is available, as discussed in Section III-B, a high packing factor is still preferred.
- In contrast to a standard inductor design, in which the required effective permeability is inversely proportional to the number of turns, the required effective permeability based on our constraints and assumptions decrease more slowly as the number of turns increases, inversely proportional to the square root of N. Because there is less bene t from an increased number of turns, we can expect small numbers of turns to work well here more often than they do in standard chokes. The core volume also decreases slowly with increased N; it is also inversely proportional to the square root of N.

B. Case 2: Fixed wire diameter; ideal permeability μ_{ideal} higher than available permeability μ_a

If the available permeability is smaller than would be ideal, the inductor is not saturated, and the core area is chosen simply to meet the inductance speci cations with the given permeability. Solving (3) for core area, and applying the calculation of length from Case 1 (12), we obtain the required core area

$$A_c = C \frac{\Delta V^2}{I_{peak}^2} \frac{k_w}{N^{\frac{3}{2}} \mu_a} \tag{19}$$

and the required core volume

$$A_c \ell_c = C \frac{\Delta V^2}{I_{peak}^2} \frac{k_w^2}{N \mu_a}. \tag{20}$$

In this case, the volume decreases faster than in Case 1 as the number of turns is increased (inversely proportional to N), which makes increasing N a more appealing strategy than it is in Case 1. This applies until saturation is reached, at which point the design reverts to Case 1, and crosses over to having the ideal permeability μ_{ideal} lower than the available permeability μ_a (Case 3 discussed below in Section III-C), at which point no further reduction in core volume is possible by increasing the number of turns. Thus we expect that in some designs, a good choice will be at the border between the cases, i.e., with the number of turns that results in (18) giving the highest available value of permeability. However, a better choice in most cases will be to simply use one turn made by passing the motor leads through the core. Since these leads have a large outer diameter d_o, increasing the choke volume is preferable to using multiple turns in terms of ease of handling. Furthermore, considering the additional length of the wire $(N-1)\ell_t$ over the length with no choke, where ℓ_t is the length of one turn, also demonstrates the advantage of single-turn designs.

TABLE I

EXAMPLE DESIGNS FOR CASE 1: FREE CHOICE OF PERMEABILITY, $N = 1$

Frame size mm	ΔV V	C nF	Leads/phase	d_o mm	$I_{cm,peak}$ A	L μH	Volume $A_c\ell_c$ cm^3	ℓ_c cm	A_c cm^2	μ_{ideal}/μ_0	Ring frequency kHz
315	187	12	1	16	5	16.7	8.6	12.3	0.7	23 515	355
400	187	20	1	30	10	7.0	13.4	23.1	0.6	22 045	426
400	187	20	2	23	10	7.0	14.3	24.6	0.6	23 529	426
450	187	25	2	30	15	3.9	15.6	32.1	0.5	20 460	511
315	322	12	1	10	5	49.8	16.0	7.7	2.1	14 697	206
400	322	20	1	23	10	20.7	30.6	17.7	1.7	16 901	247
400	322	20	2	16	10	20.7	29.6	17.1	1.7	16 368	247
450	322	25	2	23	15	11.5	35.5	24.6	1.4	15 686	297

C. Case 3: Fixed wire diameter; ideal permeability μ_{ideal} lower than available permeability μ_a

If the available permeability μ_a is larger than the ideal permeability calculated by (18), in principle, it is possible to gap the core and achieve an effective permeability equal to the ideal permeability. However, if the difference between the ideal permeability and the available permeability is small, the ideal gap would be smaller than might feasible, and would be unlikely to be worth the added expense. Thus, it is also of interest to consider design with a x ed permeability larger than ideal. The volume of such a design is given by (6), as for designs using the ideal permeability. However, the result is now a constant volume, independent of the number of turns, since the permeability is x ed. Thus, there is no reason to increase the number of turns.

To complete the design by nding core path length and area, we start by noting in (6) that an increase in permeability requires a proportional increase in volume. Starting with the design based on the ideal permeability, with length speci ed by (16) and area speci ed by (17), we need to decide how to allocate this increase in volume between length and area. Since an inductor built with a core of permeability μ_a has inductance

$$L = \frac{N^2 \mu_a A_c}{\ell_c} \tag{21}$$

an increase of ℓ_c by a factor μ_a/μ_{ideal} while also increasing μ will maintain the original inductance value, whereas increasing A_c by the same factor as the increase in μ will increase the inductance by the square of the permeability ratio $(\mu_a/\mu_{ideal})^2$. If the permeability is truly x ed at a constant μ_a, the higher inductance solution (increased A_c) would be preferred, because it further decreases ground current. However, if the permeability is a strong function of frequency, the increased inductance that results from using a larger A_c decreases the ring frequency, which further increases the permeability, which in turn further increases the required volume.

Thus, with frequency-dependent permeability, the minimum-volume design uses the same area as the ideal-permeability design, as speci ed by (17), and uses a length

$$\ell_c = \frac{\mu_a}{\mu_{ideal}} \ell_{c,\mu_{ideal}} = N \mu_a I_{peak} B_{peak} \tag{22}$$

as can be seen by substitution using (18) and (16), or from directly applying Ampere's law.

D. Case 4: Variable wire size

In the case that the inductor is not wound with the same wire used to for connection between the inverter and the machine, the wire diameter and number of turns may be selected speci cally for the inductor. Once the inductance requirement is found from (2), the design becomes similar to standard inductor design for other applications, as described in many textbooks.

IV. EXAMPLE DESIGNS

A. Drive parameters for example designs

We consider 8 different example cases based on typical values for three-phase machines with random-wound winding. The machines have 315, 400, and 450 mm frame size. Both voltage ratings 400 V and 690 V are considered. Machine supply via one motor lead per phase is assumed for the smallest, two motor leads per phase for the largest, and both case for the 400 mm frame size machine. These parameters along with the corresponding values of the operating dc bus voltage V_{dc}, the common-mode voltage step ΔV (obtained by averaging the three phases when one phase makes a transition), d_o, and typical values for C are summarized in Table II.

We take B_{peak} equal to the saturation ux density of typical nanocrystalline material at 1.2 T, packing factor $F_p = 0.5$ for one and $F_p = 0.25$ for two machine lead per phase , and we attempt to limit peak ground current to 5 A (peak-to-peak of 10 A), 10 A, and 15 A for the three machine sizes respectively.

B. Design with free choice of permeability μ

The result for a single turn design for the 315 mm 400 V machine is $L = 16.7$ μH (from (2)), volume of 8.6 cm^3 (from (15)), relative permeability $\mu/\mu_0 = 23\,515$ (from (18)), path

TABLE II

DRIVE PARAMETERS FOR EXAMPLE DESIGNS

Frame size mm	Voltage rating V	V_{dc} V	ΔV V	Leads/phase	d_o mm	C nF
315	400	560	187	1	16	12
400	400	560	187	1	30	20
400	400	560	187	2	23	20
450	400	560	187	2	30	25
315	690	966	322	1	10	12
400	690	966	322	1	23	20
400	690	966	322	2	16	20
450	690	966	322	2	23	25

length of 12.3 cm (from (16)), core area of 0.7 cm^2 (from (17)), and a ring frequency of 355 kHz (from L and C). These values, along with the corresponding values for the other seven example cases, are listed in Table I.

At a voltage transition slope of 2 kV/μs, the rise time for $V_{dc} = 560$ V is 0.28 μs, which is less than two thirds of a period for all three frame sizes. This indicates that the instantaneous rise assumption is reasonably good, as is further con rmed by simulation below (Section V).

C. Design based on an available permeability of 10 000μ_0

Although both amorphous and nanocrystalline cores are available with nominal relative permeabilities of 80 000 or more their relative permeability is typically in the range of 10 000 to 20 000 in the range of 200 to 500 kHz [13] [16]. The designs in Table I require permeabilities in this neighborhood, but often higher than what is available. Thus we need to consider Case 2, in which the available permeability μ_a is smaller than would be ideal. We rst consider a conservative assumption of an available permeability of $\mu_a = 10\,000\mu_0$. From (19) and (20), we can calculate the required area and volume as a function of the number of turns, as shown in Table III. Although the core volume decreases signi cantly for large numbers of turns ($\propto 1/N$) (Fig. 4), the wire volume and dif culty of winding go up greatly for numbers of turns greater than one. Thus single-turn designs are still likely to be the most practical choice. If necessary, the larger core needed for a single turn can be assembled from several smaller cores stacked in series.

Since the ideal permeability is also a function of the number of turns (18), the assumed permeability of 10 000 is higher than ideal for some designs in Table III, as marked with * in the table. The parameters for these designs are calculated as described in Section III-C. Note that once this point is reached, the core volume is independent of the number of turns, and so increasing the number of turns further offers no advantage.

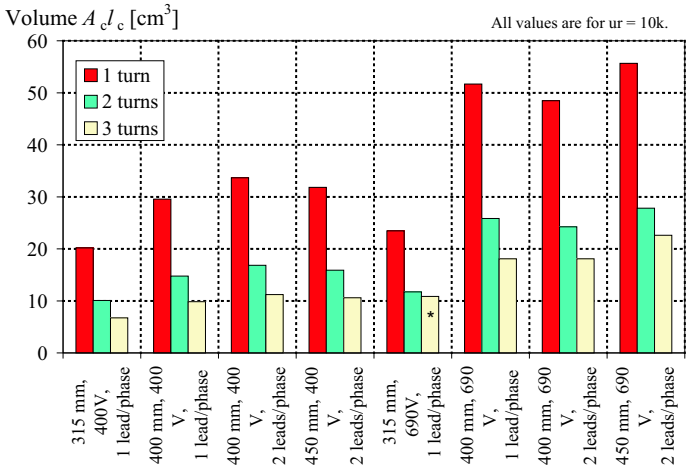

Fig. 4. Core volume $A_c\ell_c$ for different numbers of turns and available permeability of 10 000μ_0 (Table III). Most entries are calculated based on case 2: ideal μ_{ideal} higher than available μ_a; the entry marked with * has an ideal permeability below 10 000μ_0 and is calculated based on case 3: ideal μ_{ideal} lower than available μ_a.

TABLE III

EXAMPLE DESIGNS FOR CASE 2: PERMEABILITY OF 10 000μ_0 (CONSERVATIVE ASSUMPTION). MOST ENTRIES ARE CALCULATED BASED ON CASE 2: IDEAL μ_{ideal} HIGHER THAN AVAILABLE μ_a; THE ENTRIES MARKED WITH * HAVE IDEAL PERMEABILITY BELOW 10 000μ_0 AND ARE CALCULATED BASED ON CASE 3: IDEAL μ_{ideal} LOWER THAN AVAILABLE μ_a.

315 mm, 400 V, 1 lead/phase, $C = 12$ nF, $L = 16.7\,\mu$H, $d_o = 16$ mm

Number of turns, N	1	2	3	4	5
Core area, A_c, cm^2	1.64	0.58	0.32	0.21	0.15
Circumferential length, ℓ_c, cm	12.3	17.4	21.3	24.6	27.5
Core volume, $A_c\ell_c$, cm^3	20.2	10.1	6.73	5.04	4.04

400 mm, 400 V, 1 lead/phase, $C = 20$ nF, $L = 7.0\,\mu$H, $d_o = 30$ mm

Number of turns, N	1	2	3	4	5
Core area, A_c, cm^2	1.28	0.45	0.25	0.16	0.12
Circumferential length, ℓ_c, cm	23.1	32.6	40.0	46.2	51.6
Core volume, $A_c\ell_c$, cm^3	29.6	14.8	9.85	7.39	5.9

400 mm, 400 V, 2 leads/phase, $C = 20$ nF, $L = 7.0\,\mu$H, $d_o = 23$ mm

Number of turns, N	1	2	3	4	5
Core area, A_c, cm^2	1.37	0.48	0.26	0.17	0.12
Circumferential length, ℓ_c, cm	24.6	34.9	42.7	49.3	55.1
Core volume, $A_c\ell_c$, cm^3	33.7	16.8	11.2	8.4	9.7

450 mm, 400 V, 2 leads/phase, $C = 25$ nF, $L = 3.9\,\mu$H, $d_o = 30$ mm

Number of turns, N	1	2	3	4	5
Core area, A_c, cm^2	0.99	0.35	0.19	0.12	0.10*
Circumferential length, ℓ_c, cm	32.1	45.5	55.7	64.3	78.5*
Core volume, $A_c\ell_c$, cm^3	31.8	15.9	10.6	8.0	7.6*

315 mm, 690 V, 1 lead/phase, $C = 12$ nF, $L = 49.8\,\mu$H, $d_o = 10$ mm

Number of turns, N	1	2	3	4	5
Core area, A_c, cm^2	3.05	1.08	0.69*	0.52*	0.42*
Circumferential length, ℓ_c, cm	7.7	10.9	15.7*	20.9*	26.2*
Core volume, $A_c\ell_c$, cm^3	23.5	11.7	10.9*	10.9*	10.9*

400 mm, 690 V, 1 lead/phase, $C = 20$ nF, $L = 20.7\,\mu$H, $d_o = 23$ mm

Number of turns, N	1	2	3	4	5
Core area, A_c, cm^2	2.92	1.03	0.56	0.43*	0.35*
Circumferential length, ℓ_c, cm	17.7	25.0	30.7	41.9*	52.4*
Core volume, $A_c\ell_c$, cm^3	51.7	25.9	17.2	18.1*	18.1*

400 mm, 690 V, 2 leads/phase, $C = 20$ nF, $L = 20.7\,\mu$H, $d_o = 16$ mm

Number of turns, N	1	2	3	4	5
Core area, A_c, cm^2	2.83	1.00	0.54	0.43*	0.35*
Circumferential length, ℓ_c, cm	48.5	24.2	29.7	41.9*	52.4*
Core volume, $A_c\ell_c$, cm^3	17.1	24.2	16.2	18.1*	18.1*

450 mm, 690 V, 2 leads/phase, $C = 25$ nF, $L = 11.5\,\mu$H, $d_o = 23$ mm

Number of turns, N	1	2	3	4	5
Core area, A_c, cm^2	2.26	0.80	0.43	0.36*	0.29*
Circumferential length, ℓ_c, cm	24.6	34.8	42.7	62.8*	78.5*
Core volume, $A_c\ell_c$, cm^3	32.1	27.8	18.6	22.6*	22.6*

D. Design based on the permeability available at the calculated ring frequency

Given suf ciently accurate data on the permeability as a function of frequency, such as that published in [15], it is possible to do more precise design work, basing each design on the permeability available at the calculated ring frequency listed in Table I. The curves in [15] are remarkably similar for amorphous or nanocrystalline materials in the frequency range of interest, consistent with the general trends in other references [13] [16]. Depending on whether the available permeability is higher or

TABLE IV

EXAMPLE DESIGNS FOR PERMEABILITY AVAILABLE AT THE CALCULATED RING FREQUENCY, $N = 1$

Frame size mm	ΔV V	C nF	Leads/phase	d_o mm	$I_{cm,peak}$ A	L μH	Volume cm^3	ℓ_c cm	A_c cm^2	μ_a/μ_0	Ring frequency kHz
315	187	12	1	16	5	16.7	12.6	12.3	1.0	15 975	355
400	187	20	1	30	10	7.0	20.3	23.1	0.9	14 529	426
400	187	20	2	23	10	7.0	23.2	24.6	0.9	14 529	426
450	187	25	2	30	15	3.9	24.2	32.1	0.8	13 172	511
315	322	12	1	10	5	49.8	22.5	10.9	2.1	20 755	206
400	322	20	1	23	10	20.7	34.5	20.0	1.7	19 089	247
400	322	20	2	16	10	20.7	34.5	20.0	1.7	19 089	247
450	322	25	2	23	15	11.5	39.6	27.5	1.4	17 488	297

lower than the ideal permeability, the design calculations may be based on the equations in Section III-B or Section III-C. Here, only single-turns are considered because of the reasoning given previously in Section IV-C and to avoid an over o w of data. These results are shown in Table IV. Note that regardless of whether the permeability is too high or too low, the core volume ends up larger than that in the initial designs in Table I.

E. Discussion of the design results

Fig. 5 illustrates the results for the core volumes for the three designs. The gures illustrate well that:

- The smallest core volumes result from the use of the ideal permeability.
- Regardless of whether the available permeability is higher or lower than the ideal one, the core volume with the available relative permeability (Table IV) ends up larger than that in the initial design (Table I).
- The core path length ℓ_c is identical for many sets of designs because it is chosen as the smallest possible to t the wire used. The designs with longer path lengths are those in which the available permeability is higher than ideal, and the path length is increased to avoid saturation.

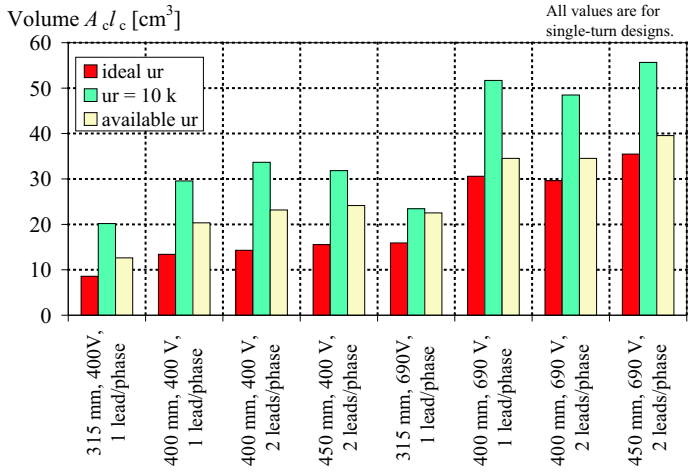

Fig. 5. Core volume $A_c\ell_c$ for ideal permeability (Table I), conservative value $\mu_a = 10\,000\mu_0$ (Table III), and permeability available at the calculated ring frequency (Table IV). All designs for $N = 1$.

V. SIMULATIONS

Transient simulations were conducted using the SIMPLIS circuit simulator [17] for the design in Table IV for a 400 V, 315 mm frame size machine. After initial simulations modelling a full three-phase system with a common-mode inductor con rmed that the ground-current behavior was identical to that of a single-phase model using the average phase voltage, simulations used a single-phase model. Simulations were conducted with several input voltage waveforms and several inductor models as described below.

Since the core permeability is not constant in the frequency range of interest, a model matching the frequency-dependent permeability in [15] was developed using a Cauer network, similar to the approach in [16], to allow a more accurate simulation. The network is shown in Fig. 6, along with the remainder of the simulated circuit, and an ideal transformer used to scale the material model to the core size and number of turns for the design in Table IV for a 400 V, 315 mm frame size machine. The frequency-dependent permeabilty, derived from the impedance of the network shown in Fig. 6, is plotted in Fig. 7. Since the rst inductor in the core network (labled L2) sees the full volt-seconds applied to the core, saturation is modelled by using a piecewise-linear inductor for that element, with abrupt saturation at 1.2 T. Simulations were also conducted with a simple ideal inductor model, also including saturation at 1.2 T.

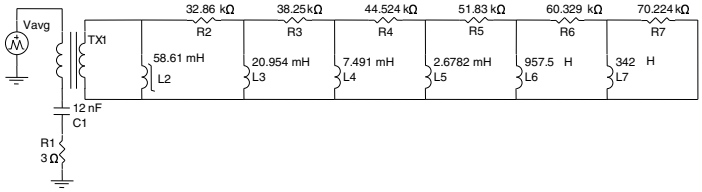

Fig. 6. Simulation model including a Cauer network to capture the effect of frequency-dependent core material.

The input voltage waveforms tested included an abrupt step with 1 ns rise time, a linear ramp corresponding to 2 kV/μs phase voltage dv/dt, and a piecewise-linear waveform that more accurately approximates an actual inverter output voltage, as shown in Fig. 8.

The results for both core models and all three input waveforms are shown in Fig. 9. The peak currents are similar to each other and are close to the 5 A design value, and all are slightly below it;

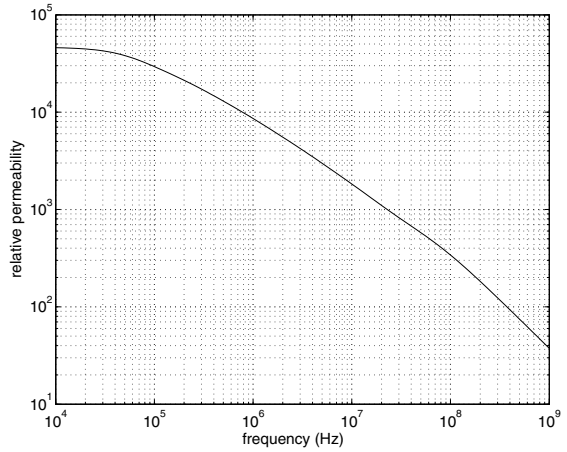

Fig. 7. Permeability calculated from the impedance of the Cauer network in 6, chosen to model typical frequency behavior of nanocrystalline materials [13] [16].

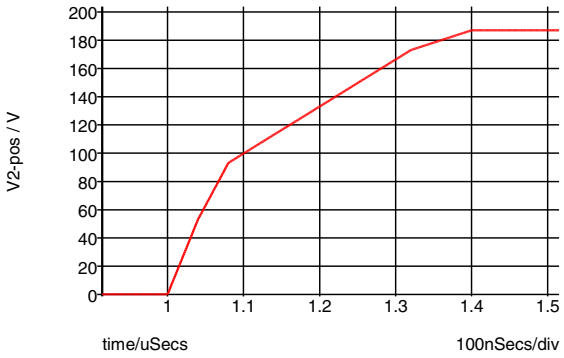

Fig. 8. Piece-wise linear voltage waveform used for simulation. This is the average voltage of three phases.

the damping which was not considered in our simpli ed design process reduces the peak current slightly. Although the peak currents and ring periods of the two inductor models are very similar, the model using a Cauer network to represent the frequency-dependent permeability has a signi cantly faster current rise time, as a result of its lower high-frequency impedance. With the ideal inductor, the shape of the voltage rise makes no discernable difference, con rming our original choice to model the input as an ideal step. With the frequency-dependent permeability, the difference are slightly more apparent, with the fastest rise time giving the highest peak, but the differences are still small.

The cores do not saturate in the simulations shown in Fig. 9. In fact, the core in the model with frequency-dependent permeability stays well below the peak ux density predicted by the design calculations. This is because the faster-than-predicted rise time accumulates a smaller integral $\int v dt$, and thus a small ux. This might indicate that more aggressive design is possible, but depending on the mechanism by which permeability is reduced at high frequency, the simple saturation model in Fig. 6 may not be accurate. Eddy current effects that reduce high-frequency permeability also concentrate the ux in the surface of the core

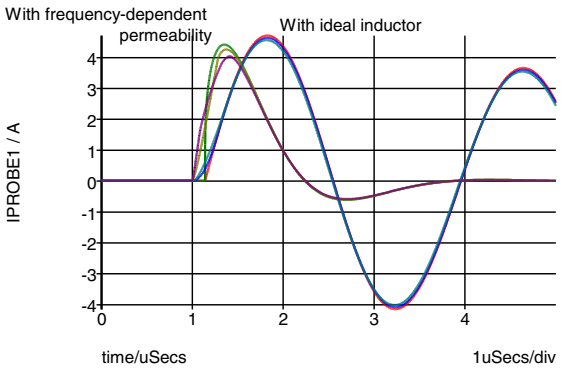

Fig. 9. Simulation of a single-turn design for a 315 mm frame size machine, using three different input waveforms with the same overall amplitude ΔV, and two different inductor models. In all cases, the current peak of ve amps matches the design speci cations well.

layers, increasing ux density for the same total ux linkage. Thus, the inductor current may be a more accurate indication of how close the real component is to saturation than the volt-second integral. By that measure, both models follow the design calculations well.

To model the saturation effects more accurately than in the presence of frequency-dependent permeability, other network topologies for the core model may be advantageous. For example, a Cauer 1 network (with series inductors and shunt resistors) can be made equivalent to the Cauer 2 network we used (with shunt inductors and series resistors) if both are linear [18], but with nonlinear elements the behaviors can be different and the Cauer 1 model may allow better capturing the effects of eddy currents on saturation [19].

VI. Conclusion

Using simplifying assumptions has allowed the development of a compact set of design equations for common-mode chokes for reducing motor ground currents. The assumptions include voltage rise time short compared to the ring period and small damping. Although these assumptions may not always be accurate, they lead to simple equations that provide insight on the effects of various parameters and allow easy design. Example designs for machines up to 450mm frame size show how effective ground-current reduction is possible with small, inexpensive, single-turn chokes.

Acknowledgment

This work was supported in part by the United States Department of Energy under grant DE-FC36-01GO1106.

References

[1] S. Chen, T. Lipo, and D. Novotny, Circulating type motor bearing current in inverter drives, *in Proceedings 31th IEEE Industry Society Annual Meeting*, vol. 1, pp. 162 167, 1996.

[2] J. Ollila, T. Hammar, J. Lisakkala, and H. Tuusa, A new reason for bearing current damanges in variable speed drives, *in Proceedings 7th European Conference on Power Electronics and Applications (EPE)*, pp. 2539 2542, Trondheim, 1997.

[3] P. Link, Minimizing electric bearing currents in ASD systems, *IEEE Industry Applications Magazine*, vol. 5, no. 4, pp. 55 66, 1999.
[4] S. Ogasawara and H. Akagi, Modeling and damping of high-frequency leakage currents in PWM inverter-fed AC motor drive systems, *IEEE Transactions in Industry Applications*, vol. 32, pp. 1105 1114, 1996.
[5] S. Ogasawara, H. Ayano, and H. Akagi, Measurement and reduction of EMI radiated by a PWM inverter-fed AC motor drive system, *IEEE Transactions in Industry Applications*, vol. 33, pp. 1019 1026, 1997.
[6] I. Boldea and S. Nasar, *Electric Drives*. CRC Press LLC, Florida, 1999.
[7] C. Mei, J. Balda, W. Waite, and K. Carr, Minimization and cancellation of common-mode currents, shaft voltages, and bearing currents for induction motor drives, *in Proceedings 34th Power Electronics Specialist Conference (PESC)*, vol. 3, pp. 1127 1132, Cape Girardeau, 2003.
[8] A. Muetze, Bearing currents in inverter-fed ac motors, Ph.D. dissertation, Darmstadt University of Technology, Shaker Verlag, Aachen, 2004.
[9] H. Akagi and T. Doumoto, Measurement and reduction of EMI radiated by a PWM inverter-fed AC motor drive system, *IEEE Transactions in Industry Applications*, vol. 40, pp. 1162 1169, 2004.
[10] A. Muetze, Scaling issues for common mode chokes to mitigate ground currents in inverter-based drive systems, *in Proceedings 40th IEEE Industry Society Annual Meeting*, vol. 3, pp. 1860 1867, Hong Kong, 2005.
[11] E. C. Snelling, *Soft Ferrites, Properties and Applications*, 2nd ed. Butterworths, 1988.
[12] R. W. Erickson and D. Maksimovie, *Fundamentals of Power Electronics*, 2nd ed. Springer, 2001.
[13] Vacuumschmelze GmbH, Nanocrystalline Vitroperm EMC components, 2004. [Online]. Available: http://www.vacuumschmelze.de
[14] Hitachi Metals, Ltd., FINEMET EMC components, 2006. [Online]. Available: http://www.hitachi-metals.co.jp/
[15] G. Herzer, *Nanocrystalline Soft Magnetic Alloys*. Elsevier Science B.V., 1997, vol. 10, ch. 3.
[16] B. Revol, H. Chazal, and J. Roudet, Common mode choke characterisation method and modelling for emi lter in power electronics, in *EPE*, 2003.
[17] Catena Software Ltd., SIMPLIS circuit simulator. [Online]. Available: http://www.catena.uk.com/
[18] G. C. Temes and J. W. LaPatra, *Introduction to circuit synthesis and design*. McGraw-Hill, 1977.
[19] P. Holmberg, A. Bergqvist, and G. Engdahl, Modelling eddy currents and hysteresis in a transformer laminate, *IEEE Transactions on Magnetics*, vol. 33, no. 2, 1997.